Delft University of Technology

Modeling and switching adaptive control for nonlinear morphing aircraft considering actuator dynamics

Xu, Wenfeng; Li, Yinghui; Lv, Maolong; Pei, Binbin

Important note
To cite this publication, please use the final published version (if applicable).
Please check the document version above.

Modeling and switching adaptive control for nonlinear morphing aircraft considering actuator dynamics

Wenfeng Xu [a], Yinghui Li [b], Maolong Lv [b,c], Binbin Pei [b,∗]

[a] *Graduate College, Air Force Engineering University, Xi'an 710038, China*
[b] *Aeronautics Engineering College, Air Force Engineering University, Xi'an 710038, China*
[c] *Faculty of Aerospace Engineering, Delft University of Technology, Mekelweg 2, Delft 2628CD, the Netherlands*

A B S T R A C T

This paper investigates the problems of modeling and control of the morphing aircraft. Henceforth, a nonlinear dynamic model of a wing-sweep morphing aircraft is first established in this work. This model is suitable for larger envelopes by elaborating the variation of aerodynamic coefficients, air density, mass distribution at different altitudes, Mach numbers, and sweep angles. Considering the alterations in the dynamic characteristics of the morphing aircraft owing to the various flight conditions, we design the switching adaptive backstepping controllers for the altitude subsystem and velocity subsystem. The actuator dynamics have been explicitly included in the process of the controller design to alleviate the chattering problem caused by the switching. Furthermore, the closed-loop stability is rigorously proved via the Lyapunov stability theory and the technique of compact set. Comparative results from the simulations finally validate the effectiveness of the proposed scheme.

© 2022 Elsevier Masson SAS. All rights reserved.

1. Introduction

Morphing aircrafts are flight vehicles that can change their aerodynamic shape to adapt to different environments and missions [1]. It has attracted tremendous attention from the academia and engineering fields owing to its ability to accomplish multi-objective and multi-task [2,3]. Most of the literature concerning morphing aircraft has been focused on morphing structures and materials [4–6], aerodynamic performance analysis [7–10]. Nevertheless, certain obstacles need to be overcome in the modeling and control of morphing aircraft [3]. High-performance flight control system is required to maintain the stability during the morphing process. However, altering the aerodynamic shape produces the time-varying effect of the aerodynamic coefficients and extra inertial force, which incurs tremendous difficulties to the design of flight control system. Being one of the critical techniques for the morphing aircraft, the design of the flight control system during the wing transition process is attracting widespread interest in the fields such as control engineering, aviation, and machinery.

Linear systems have been first utilized to model morphing aircrafts in [11–19], based on which, several control methodologies have been formulated. For example, in [11,12], linear quadratic regulators (LQR) have been used to determine optimal control laws minimizing the quadratic performance measure. In [13], the switching proportional-integral-derivative (PID) controllers have been devised in accordance with the six different morphing configurations. However, the variation of the mass distribution and aerodynamic coefficients, even at the same altitude and Mach numbers during morphing, indicates the conservativeness of the LTI models. Consequently, linear parameter-varying (LPV) models have been exploited to overcome the above-mentioned drawback [14–16]. The non-switching LPV model is originally obtained from the convex combination of a set of LTI models [17], and the tensor product (TP) modeling method has been developed to reduce the computational burden of the modeling [18]. To ensure the feasibility of the LPV controller, the switching LPV controller has been proposed to replace the non-switching controller [20,21]. In [22], the switching polytopic linear parameter-varying controller has been used for morphing the aircraft in full envelope, and the mode-dependent average dwell time (MDADT) switching logics has been proposed to improve the properties of both the robustness and computational complexity. However, it should be noted that the LPV system cannot accurately describe the morphing aircraft dynamics since it neglects some important nonlinear characteristics, such as the fast changes of the aerodynamics during the transitions between different flight conditions.

Subsequently, several control methodologies have been formulated based on a nonlinear model of the morphing aircraft. For instance, in [23], a nonlinear controller based on the dynamic inversion has been proposed, with feed-forward off-line neural networks being utilized for the model inversion. Unfortunately, the dynamic inversion method necessitates the model to be known completely, and the errors caused by the model uncertainties may be relatively large. The sliding mode control has stronger robustness, and hence, a multi-loop sliding mode controller has been designed for the time-vary nonlinear model of the morphing aircraft in [24], besides presenting an adaptive super-twisting algorithm sliding mode method to improve the tracking performance and the robustness of the controller [25]. However, the chattering issue appearing in the sliding mode control is challenging to solve. Another common nonlinear method is the adaptive control. In [26,27], an adaptive back-stepping controller has been devised, and the dynamics of the morphing aircraft have been approximated by the radial basis function neural networks. The primary drawback of this method is that the variation of the mass distribution and aerodynamic coefficients caused by the morphing cannot always be accurately approximated by the neural networks, which constrains the control performance of this type of method.

To balance the complexity and accuracy of the modeling, the theory of switched nonlinear system has been applied to the modeling and control of the morphing aircraft [28], and the morphing aircraft is modeled as a switched nonlinear system. Further, the adaptive dynamic programming method has been employed to generate an additional control input for the purpose of improving the tracking accuracy [29]. Although it is convenient to use the switched nonlinear system to describe the parameter variation of the morphing aircraft, it does not capture the behavior of the continuous dynamics of the morphing aircrafts in the real world. Consequently, the nonlinear switched system modeling method is not accurate enough, which will lead to certain conservativeness in the controller design. On the other hand, most of the nonlinear model-based controllers in the previous works did not consider the variation of the morphing aircraft parameters with the altitudes and Mach numbers, which makes the controller unsuitable for larger envelopes. It should be noted that good performance under multiple flight conditions is one of the main advantages of the morphing aircraft. Therefore, it is essential to take the different flight conditions into account during the modeling and controller design.

In this paper, the dynamic characteristics of a morphing aircraft under different configurations, altitudes, and Mach numbers have been studied, so that a nonlinear morphing aircraft model more suitable for larger envelopes is established. Further, the longitudinal model is decomposed into the altitude and velocity subsystems. Inspired by [30–33], the switching back-stepping adaptive controllers have been designed for the altitude and velocity subsystems. The primary contributions of this paper, with respect to the relevant literature, have been summarized in the following.

(1) In contrast with [28,29], a continuous nonlinear dynamic model combined with the switching controllers has been used instead of a switching model during the controller design and stability analysis, which can describe the dynamic characteristics more accurately than switching model. Furthermore, the variation of the aerodynamic parameters at different altitudes and Mach numbers is considered in the modeling process, which makes the proposed model suitable for larger envelopes. Further, it better reflects the original intention of the morphing aircraft to pursue the optimal performance under various flight conditions.
(2) Compared with the non-switching back-stepping controller described in [26] and [27], a switching back-stepping controller has been designed in this work, which has better tracking performance. The switching of the control laws produces instantaneous jumping of the Lyapunov function, which incurs difficulties in the stability analysis. Inspired by [34], the invariant set theory has been applied to handle the possible jumping of the value of Lyapunov function and to facilitate stability analysis.
(3) Unlike [26–29], we consider the actuator dynamics throughout the control design and stability analysis processes, which alleviates the chattering problem possibly induced by the fast change of the command signals.

2. Modeling of morphing aircraft

2.1. Equations of motion of morphing aircraft

According to the results in [35], the equations of motion for the general morphing aircraft can be expressed in a vector form

$$\boldsymbol{F} = m\dot{\boldsymbol{v}} - \boldsymbol{S}\dot{\boldsymbol{w}} + m\left(\boldsymbol{w} \times \boldsymbol{v}\right) - \left(\boldsymbol{w} \times \boldsymbol{S} + 2\dot{\boldsymbol{S}}\right)\boldsymbol{w} + \int \ddot{\boldsymbol{\rho}}_i dm_i, \tag{1}$$

$$\boldsymbol{M} = \boldsymbol{S}\dot{\boldsymbol{v}} + \boldsymbol{J}\dot{\boldsymbol{w}} + \boldsymbol{S}\left(\boldsymbol{w} \times \boldsymbol{v}\right) + \boldsymbol{w} \times \left(\boldsymbol{J}\boldsymbol{w}\right) - 2\int \boldsymbol{\rho}_i \times \left(\dot{\boldsymbol{\rho}}_i \times \boldsymbol{w}\right) dm_i + \int \boldsymbol{\rho}_i \times \ddot{\boldsymbol{\rho}}_i dm_i, \tag{2}$$

where $\boldsymbol{F}$ and $\boldsymbol{M}$ are the total applied force and moment, respectively. Further, m is the mass of the aircraft, and $\boldsymbol{S}$ and $\boldsymbol{J}$ are the static moment and inertia matrix of the aircraft, respectively, about O_b (origin of body coordinates). $\boldsymbol{w} = \begin{bmatrix} p & q & r \end{bmatrix}^{\mathrm{T}}$ is the angular velocity vector; $\boldsymbol{v} = \begin{bmatrix} u & v & w \end{bmatrix}^{\mathrm{T}}$ is the velocity vector; $\boldsymbol{\rho}_i = \begin{bmatrix} \rho_{xi} & \rho_{yi} & \rho_{zi} \end{bmatrix}^{\mathrm{T}}$ is the position vector relative to O_b of each particle in the whole aircraft, and m_i is the mass of each particle (cf. Fig. 1).

Assumption 1. [25] There are only symmetrical morphing of the wings and longitudinal movement in the aircraft, and O_b is located at the center of the mass of the rigid and nondeformable fuselage.

Remark 1. The symmetric morphing ensures the lateral unbalanced force and moment will not be generated. On the other hand, the location of the O_b guarantees that the static moment of the wing is equal to that of the whole aircraft.

Let $\boldsymbol{\rho}_i^{\boldsymbol{w}} = \begin{bmatrix} \rho_{xi}^w & \rho_{yi}^w & \rho_{zi}^w \end{bmatrix}^{\mathrm{T}}$ denote the position vector of each particle in the wings. It follows from Assumption 1 that

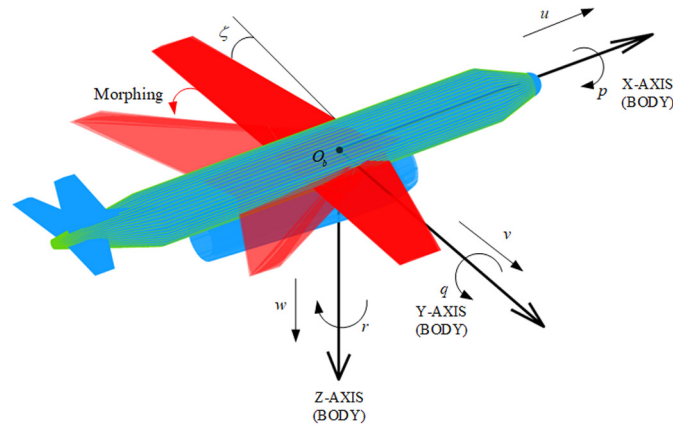$$\int \boldsymbol{\rho}_i dm_i = \int \boldsymbol{\rho}_i^{\boldsymbol{w}} dm_i, \tag{3}$$

Fig. 1. Definitions of axes and motions.

$$\int \rho_{y_i}^w dm_i = \int \rho_{z_i}^w dm_i = 0, \tag{4}$$

$$p = r = v = 0. \tag{5}$$

According to the coordinate transformation between the wind and body axes [36], the following equations hold.

$$\mathbf{w}^s = A_{s/b} \mathbf{w}$$
$$= \begin{bmatrix} \cos\alpha & 0 & \sin\alpha \\ 0 & 1 & 0 \\ -\sin\alpha & 0 & \cos\alpha \end{bmatrix} \begin{bmatrix} p \\ q \\ r \end{bmatrix} = \begin{bmatrix} p\cos\alpha + r\sin\alpha \\ q \\ -p\sin\alpha + r\cos\alpha \end{bmatrix}, \tag{6}$$

$$\mathbf{v} = A_{b/s} \mathbf{v}^s$$
$$= \begin{bmatrix} \cos\alpha & 0 & -\sin\alpha \\ 0 & 1 & 0 \\ \sin\alpha & 0 & \cos\alpha \end{bmatrix} \begin{bmatrix} V_T \\ 0 \\ 0 \end{bmatrix} = \begin{bmatrix} V_T\cos\alpha \\ 0 \\ V_T\sin\alpha \end{bmatrix}. \tag{7}$$

Separating (1) and (2) into the stability and body axes, respectively, and combining with (3)-(7), the equations of motion can be represented by

$$\dot{V} = \frac{1}{m}(T\cos\alpha - D - mg\sin\gamma + H_x\cos\alpha + H_z\sin\alpha),$$
$$\dot{\gamma} = \frac{1}{Vm}(T\sin\alpha + L - mg\cos\gamma + H_x\sin\alpha - H_z\cos\alpha), \tag{8}$$
$$\dot{q} = (M_A + M_F - S_x g\cos\theta + TZ_T)/J_y,$$

where $S_x = \int \rho_{xi}^w dm_i$, $J_y = \int \rho_{xi}^{w2} + \rho_{zi}^{w2} dm_i$, $H_x = (-\ddot{S}_x + Q^2 S_x)$, $H_z = (2Q\dot{S}_x + \dot{Q}S_x)$, $M_F = S_{x1}(\dot{V}\sin\alpha - V\cos\alpha\dot{\gamma}) - \dot{J}_y q$. Drag, lift, and pitching moment are formulated as

$$D \approx \bar{q}S_w(\zeta)\left(C_D^{\alpha^2}(\zeta,V,h)\alpha^2 + C_D^{\alpha}(\zeta,V,h)\alpha + C_D^0(\zeta,V,h)\right),$$

$$L \approx L_\alpha\alpha + L_0\alpha = \bar{q}S_w(\zeta)\left(C_L^{\alpha}(\zeta,V,h)\alpha + C_L^0(\zeta,V,h)\right),$$

$$M_A \approx M_{A\alpha} + M_{A0} + M_{A\delta_e}\delta_e + M_{Aq}\frac{qc_A(\zeta)}{2V}$$

$$= \bar{q}S_w(\zeta)c_A(\zeta)\left(C_M^{\alpha}(\zeta,V,h)\alpha + C_M^0(\zeta,V,h) + C_M^{\delta_e}(\zeta,V,h)\delta_e + \frac{C_M^q(\zeta,V,h)qc_A(\zeta)}{2V}\right),$$

where $\bar{q} = \frac{1}{2}\rho(h)V^2$ is the dynamic pressure, $\rho(h)$ is the air density, S_w is the wing area, and c_A is the mean aerodynamic chord.

To obtain the values of c_A, S_w, J_y, and S_x at the specific the sweep angle ζ, these parameters at $\zeta = 16°, 25°, 35°, 45°, 55°, 60°$ are selected to generate one-dimensional tables as a function of the sweep, which are given in [13]. Further, the values of these parameters can be interpolated from these tables.

Remark 2. The equation of motion (8) is different from the rigid aircraft owing to the change of the shape and mass distribution caused by the morphing. The shape changes affect the wing parameters c_A, S_w, and the aerodynamic coefficients, viz., C_L, C_D, and C_M. The variation of mass distribution affects the inertial parameters of the aircraft, viz., S_x and J_y, and the position of the center of gravity (CG). The movement of CG invokes additional inertial force H_x, H_z and inertial moment M_F, and it affects C_M by changing the magnitude of the moment arm.
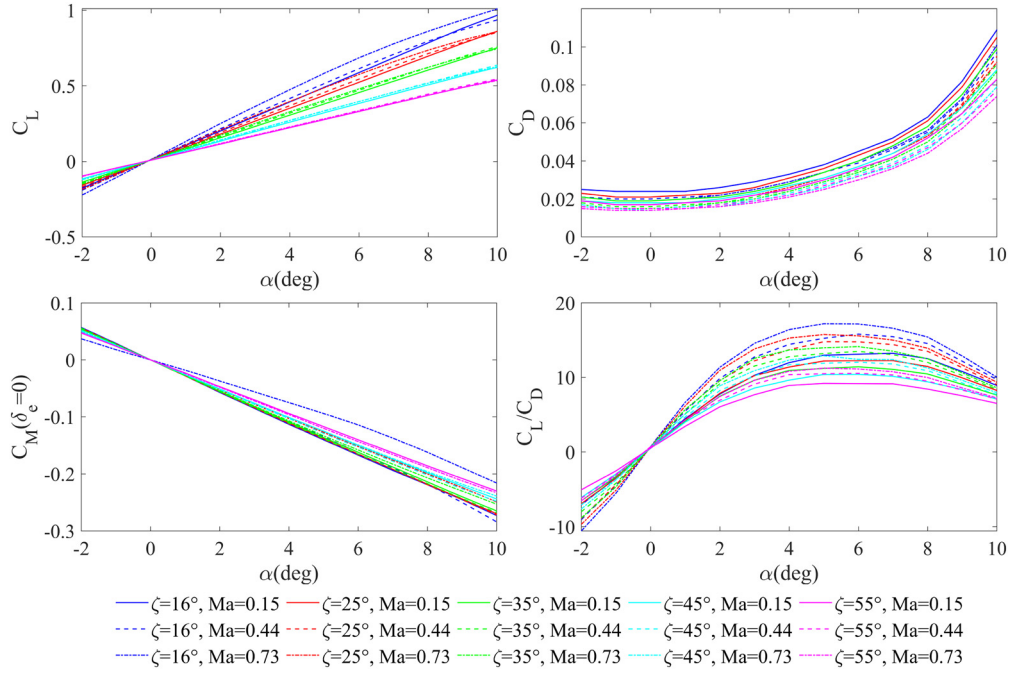
Fig. 2. Aerodynamic coefficient for $h = 3000$ m.

2.2. Aerodynamic analysis

To acquire the accurate longitudinal nonlinear model, we need to obtain the complete aerodynamic data of the aircraft. There are primarily three methods to obtain the aerodynamic coefficients according to the literature, including CFD [7,8,10], Finite Element Analysis [9], DATCOM [13,25], and wind tunnel test [24]. The aerodynamic analysis in this paper is based on [13], and we extend the work to different conditions of Mach numbers and altitude. Aerodynamic derivatives at different sweep angles, altitudes, and Mach numbers have been obtained by DATCOM, and the geometric and inertial parameters of each configuration can be found in [13]. The aerodynamic derivatives obtained by DATCOM have been used to generate three-dimensional look-up tables, and the interpolation is used to construct the aerodynamic derivatives during the transition.

According to Fig. 2, for positive values of the angle of attack, the lift and drag coefficients are positively correlated with the sweep angle and negatively correlated with the Mach number. When the angle of attack is negative, they are negatively correlated with the sweep angle and positively correlated with the Mach number. The pitching coefficients decrease with the increasing sweep angle under a positive angle of attack. This owes to the increased magnitude of the moment arm contributing less to the pitching moment than the decrease of the reduced magnitude of lift. The Mach number has a significant impact on the aerodynamic coefficients, especially in the case of a small sweep angle. Mach number is therefore considered as an essential parameter in the following sections.

According to Fig. 3, the lift-to-drag ratio decreases slightly with the increase of altitude, and the rate of decline further decreases with velocity. The variation of the air density with the altitude is more significant than that of the lift-drag ratio, and the relationship between the altitude and air density is estimated as $\rho(h) = \rho_0 \exp(-h/h_s)$ [37], where ρ_0 is the nominal air density at sea level and h_s^{-1} is the air density decay rate. Obviously, with the increase of altitude, a larger angle of attack is required to generate sufficient lift, and the variation of the angle of attack changes the pitching moment M_A and the inertia moment M_F. Hence, the morphing aircraft have different dynamic characteristics at different altitudes. Therefore, it is inevitable to consider the altitude in the modeling and controller design to improve the accuracy of the model and the performance of the controller.

2.3. Model transformation

Assumption 2. The flight path angle γ is small, i.e., $\sin\gamma \approx \gamma$.

Similar to [25–28], the longitudinal model is decomposed into the velocity and altitude subsystems.
The altitude subsystem can be written as

$$
\begin{aligned}
\dot{h} &= V\gamma, \\
\dot{\gamma} &= f_\gamma + g_\gamma\theta + d_\gamma, \\
\dot{\theta} &= q, \\
\dot{q} &= f_q + g_q\delta_e + d_q,
\end{aligned}
\tag{9}
$$

where $f_\gamma = \frac{L_0 - L_\alpha\gamma}{mV} - \frac{g}{V}cos\gamma$, $g_\gamma = \frac{L_\alpha}{mV}$, $f_q = \frac{M_{A\alpha}\alpha + M_{A0}}{J_y} + \frac{M_{Aq}qc}{2J_yV}$, $g_q = \frac{M_{A\delta_e}}{J_y}$, $d_\gamma = \frac{T\sin\alpha + H_x\sin\alpha - H_z\cos\alpha}{mV} + d_{\Delta\gamma}$, $d_q = TZ_T + M_F - \dot{J}_yq + d_{\Delta q}$. Further, $d_{\Delta\gamma}$ and $d_{\Delta q}$ denote the equivalent disturbances caused by model uncertainties and unmodeled terms. The dynamics of the elevator are approximately modeled as the first-order dynamic system, given as
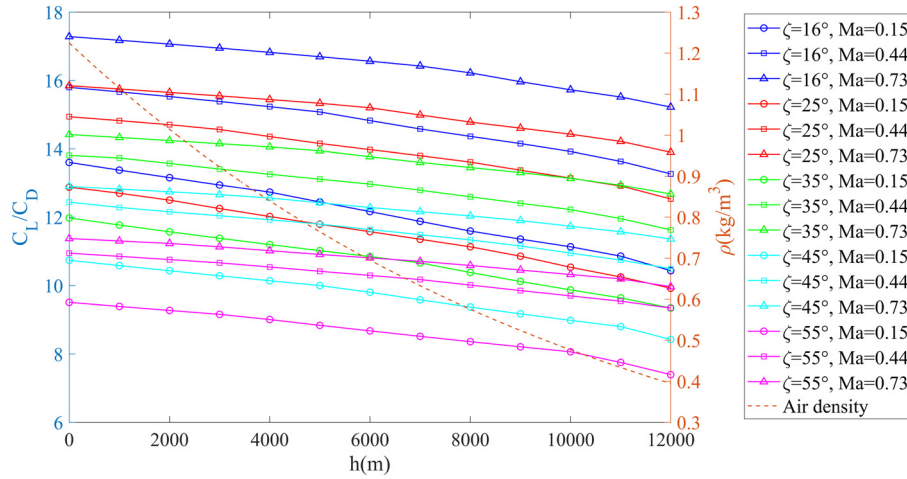
Fig. 3. Variation of the air density and lift-drag ratio with altitude.

$$\dot{\delta}_e = \frac{1}{T_\delta} \left(\delta_{cm} - \delta_e \right).$$

On the other hand, we express the velocity subsystem as

$$\dot{V} = f_v + g_v T + d_v, \tag{10}$$

where $f_v = \frac{1}{m} \left(-D - mg \sin \gamma \right)$, $g_v = \frac{\cos \alpha}{m}$, $d_v = H_x \cos \alpha + H_z \sin \alpha + d_{\Delta v}$, in which $d_{\Delta v}$ denote the equivalent disturbances caused by the model uncertainties and unmodeled terms, and the dynamics of the engine is also modeled as the first-order dynamic system as

$$\dot{T} = \frac{1}{T_T} \left(T_{cm} - T_e \right).$$

Assumption 3. [29] The disturbance d_γ, d_q and d_v are bounded and differentiable. i.e., there exist positive constants $\bar{d}_l$ and $\bar{\bar{d}}_l, l = \gamma, q, v$, such that $|d_l| \leq \bar{d}_l$, $|\dot{d}_l| \leq \bar{\bar{d}}_l$.

Assumption 4. The velocity reference signal V_r is first-order differentiable and bounded, and the altitude reference signal h_r is second-order differentiable and bounded.

3. Controller design

3.1. Switching principle of the controller

According to the equations of motion and aerodynamic analysis, the aerodynamic parameters of the morphing aircraft vary widely under different altitudes, Mach numbers, and sweep angles, which make it challenging to find a global controller with good performance. To solve this problem, the idea of gain scheduling has been introduced into the backstepping adaptive control. The state-space of the scheduling parameters $[h, \mathrm{Ma}, \zeta]$ has been partitioned into different sub-intervals, as shown in Fig. 4. For each sub-interval, different control laws are designed, and $f_\gamma, f_q, f_v, g_\gamma, g_q$ are estimated according to the aerodynamic coefficients of the nearby working points in Section 2.2, denote as $f_\gamma^\sigma, f_q^\sigma, f_v^\sigma, g_\gamma^\sigma, g_q^\sigma$, respectively. The switching rule of the controller is decided by the sub-interval to which the real-time scheduling parameters belong.

Remark 3. In Fig. 4, the division of sweep angles is based on several typical configurations in [13], and the division of Mach numbers is to divide the envelope into low speed, medium speed, and high speed zones. The reason for segregating the altitude values by an interval of 1000 m is that the air density decreases by about 10% for every altitude increment of 1000 m. On the other hand, the level of detail of the envelope division is a compromise between the tracking accuracy in each sub-interval and the number of switches. A high level of detail of the envelope division is beneficial for improving the tracking accuracy in each sub-interval, but it leads to the frequent switching of the control laws that is detrimental to the fast convergence of the system. The designing of a smoother switching nonlinear controller, intended to diminish this compromise, will be pursued in our future research.

Assumption 5. In the process of controller operation, there exists a positive constant $\beta_i \in \left(0, \frac{1}{2} \right)$ such that $\left| g_i - g_i^\sigma \right| \leq \beta_i \left| g_i \right|$ for $i = \gamma, q$.

Remark 4. In this paper, $f_\gamma, f_q, f_v, g_\gamma, g_q$ are assumed to be unknown. Assumption 5 implies that the relative error of our estimates of g_γ and g_q is within 50%, which is useful to the stability analysis.
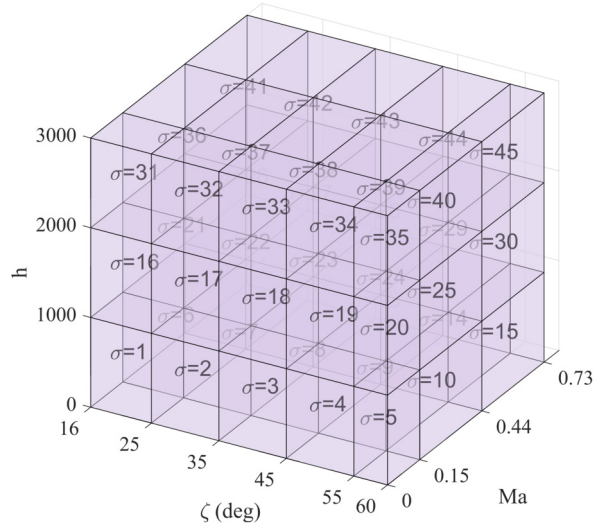
Fig. 4. The switching rule of the controller.

3.2. Technical tools

This section introduces several lemmas that are instrumental in deriving the main results of this paper.

Lemma 1. [38] *For any positive constant ε, the inequality*

$$|x| - x\tanh\left(\frac{cx}{\varepsilon}\right) \le \varepsilon, c = 0.2785$$

holds for any $x \in \mathbb{R}$.

Lemma 2. [39] *For any positive constant k_b, the inequality*

$$\ln\left(\frac{k_b{}^2}{k_b{}^2 - z^2}\right) < \frac{k_b{}^2}{k_b{}^2 - z^2}$$

holds for any z in the interval $|z| \le k_b$.

Lemma 3. [40] *For any positive constant k_b, let $Z_1 = \{z_1 \in \mathbb{R} : |z_1| < k_b\} \subset \mathbb{R}$ and $N = \{\mathbb{R}^l \times Z_1\} \subset \mathbb{R}^{l+1}$ be open sets. Consider the system $\dot{\eta} = h(t, \eta)$, where $\eta = [w, z_1]^T \in N$ is the state and the function $h : \mathbb{R}_+ \times N \to \mathbb{R}^{l+1}$ is piecewise continuous in t and locally Lipschitz in z_1, uniformly in t on $\mathbb{R}_+ \times N$. Suppose that there exist continuously differentiable and positive definite functions $U : \mathbb{R}^l \to \mathbb{R}_+$ and $V : Z_1 \to \mathbb{R}_+$ such that*

$$V_1(z_1) \to \infty \text{ as } |z_1| \to k_b$$
$$\gamma_1(\|w\|) \le U(w) \le \gamma_2(\|w\|)$$

with γ_1, γ_2 as κ_∞ functions. Let $V(\eta) = V_1(z_1) + U(w)$, and $z_1(0) \in Z_1$, if the inequality holds

$$\dot{V} \le -\mu V + \lambda$$

in the set $\eta \in N$ and μ, λ positive constants, then w remains bounded and $z_1(t) \in Z_1, \forall t \cup [0, \infty)$.

3.3. Altitude controller design

Define the tracking errors as $e_1 = h - h_r$, $e_2 = \gamma - \alpha_{c1}$, $e_3 = \theta - \alpha_{c2}$, $e_4 = q - \alpha_{c3}$ and $e_5 = \delta_a - \alpha_{c4}$, where α_{ci} is the output of the first-order filter with the virtual control law α_i^σ as the input as given below,

$$\dot{\alpha}_{ci} = \frac{1}{\tau_i}\left(\alpha_i^\sigma - \alpha_{ci}\right), \alpha_i(0) = \alpha_{ci}^\sigma(0). \tag{11}$$

Define the filter error $z_{i+1} = \alpha_i^\sigma - \alpha_{ci}$.

Remark 5. The introduction of the first-order filter circumvents the 'explosion of complexity' in the sense that the derivative of virtual control law is estimated by the output of the filter, and smoothens the command signals in the sense that the output of the filter changes continuously. The latter point can be observed from the results of the simulation in this paper.

Step 1: Choose the Lyapunov function as $L_{h1} = \frac{1}{2}e_1^2$, and taking the derivative of L_{h1} yields

$$\dot{L}_{h1} = e_1(\dot{h} - \dot{h}_r) = e_1[V(\alpha_1^\sigma + z_2 + e_2) - \dot{h}_r], \tag{12}$$

and designing the virtual control law as

$$\alpha_1^\sigma = (-k_1^\sigma e_1 + \dot{h}_r)/V. \tag{13}$$

Then, substituting Eq. (13) into (12) yields

$$\dot{L}_{h1} = -k_1^\sigma e_1^2 + e_1(e_2 + z_2).$$

Step 2: Choose the Lyapunov function as $L_{h2} = L_{h1} + \frac{1}{2}e_2^2$, and taking the derivative of L_{h2} arrives at

$$\begin{aligned}
\dot{L}_{h2} &= \dot{L}_{h1} + e_2(\dot{\gamma} - \dot{\alpha}_{c1}) \\
&= \dot{L}_{h1} + e_2[f_\gamma^\sigma + g_\gamma^\sigma(\alpha_2^\sigma + e_3 + z_3) \\
&\quad + (g_\gamma - g_\gamma^\sigma)(\alpha_2^\sigma + e_3 + z_3) + \Delta_\gamma^\sigma + d_\gamma - \dot{\alpha}_{c1}],
\end{aligned} \tag{14}$$

where $\Delta_\gamma^\sigma = f_\gamma^\sigma - f_\gamma$, whereas designing the virtual control law as

$$\alpha_2^\sigma = \frac{1}{g_\gamma^\sigma}\left[-k_2^\sigma e_2 + \dot{\alpha}_{c1} - f_\gamma^\sigma - \hat{D}_\gamma \tanh\left(\frac{ce_2\hat{D}_\gamma}{\varepsilon_V}\right) - Ve_1\right], \tag{15}$$

in which $\hat{D}_\gamma$ is adapted by

$$\dot{\hat{D}}_\gamma = |e_2| - k_{D\gamma}\hat{D}_\gamma. \tag{16}$$

Then, combining (14)-(16) and Assumption 5 yields

$$\begin{aligned}
\dot{L}_{h2} &\leq \dot{L}_{h1} - k_2^\sigma e_2^2 + e_2(d_\gamma + \Delta_\gamma) + g_\gamma^\sigma e_2(z_3 + e_3) - \hat{D}_\gamma e_2 \tanh\left(\frac{c\hat{D}_\gamma e_2}{\varepsilon_V}\right) \\
&\quad - Ve_1e_2 + \left|e_2\lambda_\gamma g_\gamma^\sigma\right||\alpha_2 + e_3 + z_3| \\
&\quad - Ve_1e_2 + \lambda_\gamma\left|-k_2^\sigma e_2^2 + e_2\dot{\alpha}_{c1} - e_2 f_\gamma^\sigma - e_2\hat{D}_\gamma \tanh\left(\frac{ce_2\hat{D}_\gamma}{\varepsilon_V}\right) - Ve_1e_2 + g_\gamma^\sigma e_3 + g_\gamma^\sigma z\right| \\
&\leq \dot{L}_{h1} - k_2^\sigma(1 - \lambda_\gamma)e_2^2 + |e_2|D_\gamma^\sigma + g_\gamma^\sigma e_2(z_3 + e_3) - \hat{D}_\gamma e_2 \tanh\left(\frac{c\hat{D}_\gamma e_2}{\varepsilon_V}\right) \\
&\quad - Ve_1e_2 + \lambda_\gamma\left|e_2\hat{D}_\gamma \tanh\left(\frac{ce_2\hat{D}_\gamma}{\varepsilon_V}\right)\right|,
\end{aligned}$$

where $\lambda_\gamma = \frac{\beta_\gamma}{1-\beta_\gamma}$.

Step 3: Choose the Lyapunov function as $L_{h3} = L_{h2} + \frac{1}{2}e_3^2$, and by taking the derivative of L_{h3}, we obtain

$$\dot{L}_{h3} = \dot{L}_{h2} + e_3(\dot{\theta} - \dot{\alpha}_{c2}) = \dot{L}_{h2} + e_3[(\alpha_3^\sigma + e_4 + z_4) - \dot{\alpha}_{c2}], \tag{17}$$

and thus, designing the virtual control law as

$$\alpha_3^\sigma = -k_3^\sigma e_3 + \dot{\alpha}_{c2} - g_\gamma^\sigma e_2. \tag{18}$$

Substituting Eq. (18) into (17) yields

$$\dot{L}_{h3} = \dot{L}_{h2} - k_3^\sigma e_3^2 - g_\gamma^\sigma e_2 e_3 + e_3(e_4 + z_4).$$

Step 4: Choose the Lyapunov function as $L_{h4} = L_{h3} + \frac{1}{2}e_4^2$, and the derivative of L_{h4} leads to

$$\begin{aligned}
\dot{L}_{h4} &= \dot{L}_{h3} + e_4[f_q^\sigma + g_q^\sigma(\alpha_4^\sigma + e_5 + z_5) \\
&\quad + (g_q - g_q^\sigma)(\alpha_4^\sigma + e_5 + z_5) + \Delta_q^\sigma + d_q - \dot{\alpha}_{c3}],
\end{aligned} \tag{19}$$

where $\Delta_q^\sigma = f_q^\sigma - f_q$. Design the virtual control law as

$$\alpha_4^\sigma = \frac{1}{g_q^\sigma}\left[-k_4^\sigma e_4 + \dot{\alpha}_{c3} - f_q^\sigma - \hat{D}_q \tanh\left(\frac{ce_4\hat{D}_\gamma}{\varepsilon_V}\right) - e_3\right], \tag{20}$$

where $\hat{D}_q$ is adapted by

$$\dot{\hat{D}}_q = |e_4| - k_{Dq}\hat{D}_q. \tag{21}$$

Then, combining Eqs. (19)-(21) with Assumption 5 yields

$$
\begin{aligned}
\dot{L}_{h4} \leq{} & \dot{L}_{h3} - k_4^\sigma e_4^2 + e_4\left(d_q + \Delta_q\right) + g_q^\sigma e_4 \left(z_5 + e_5\right) - \hat{D}_q e_4 \tanh\left(\frac{c\hat{D}_q e_4}{\varepsilon_V}\right) - e_3 e_4 \\
& + \lambda_q \left| -k_4^\sigma e_4^2 + e_4 \dot{\alpha}_{cc} - e_4 f_q^\sigma - e_4 \hat{D}_q \tanh\left(\frac{c e_4 \hat{D}_q}{\varepsilon_V}\right) - e_3 e_4 + e_4 e_5 + e_4 z_5 \right| \\
\leq{} & \dot{L}_{h3} - k_4^\sigma \left(1 - \lambda_q\right) e_4^2 + |e_4|\, D_q^\sigma + g_q^\sigma e_4 \left(z_5 + e_5\right) \\
& - \hat{D}_q e_4 \tanh\left(\frac{c\hat{D}_q e_4}{\varepsilon_V}\right) - e_3 e_4 + \lambda_q \left| e_4 \hat{D}_q \tanh\left(\frac{c e_4 \hat{D}_q}{\varepsilon_V}\right)\right|,
\end{aligned}
$$

where $\lambda_q = \frac{\beta_q}{1 - \beta_q}$.

Step 5: Choose the Lyapunov function as

$$L_{h5} = L_{h4} + \frac{1}{2}\log\frac{k_h^2}{k_h^2 - e_5^2}, \tag{22}$$

and taking the derivative of Eq. (22) results in

$$\dot{L}_{h5} = \dot{L}_{h4} + \frac{e_5}{k_h^2 - e_5^2}\left[\frac{1}{T_a}\left(\delta_e - \delta_a\right) - \dot{\alpha}_{c4}\right],$$

and then, design the control law as

$$\delta_e = \delta_a + T_a\left[-k_5 e_5^2 + \dot{\alpha}_{c4} - \left(k_h^2 - e_5^2\right)g_q^\sigma e_4\right]. \tag{23}$$

Then

$$\dot{L}_{h5} = \dot{L}_{h4} + \frac{k_5 e_5^2}{k_h^2 - e_5^2} - g_q^\sigma e_4 e_5.$$

Assumption 6. The controller can only switch a limited number of times in a finite time, i.e., Zeno behavior will not occur [41], and the minimum dwell time of the mode of the controller is denoted as μ_m.

Theorem 1. *Consider the closed-loop system composed by (9), by the control laws (13), (15), (18), (20), (23), and by the adaptive laws (16), (21), let Assumptions 1-6 hold. Given any initial error condition $|e_5(0)| < k_h$, then there exist a set of design parameters, such that all signals of the closed-loop system remain bounded, and the altitude tracking error e_1 will converge to a small neighborhood of the origin determined by the design parameters. Furthermore, e_5 will remain in the set $|e_5| < k_h$.*

Proof. Consider the compact set

$$
\begin{aligned}
A &= A_e \times A_D \times A_h \\
&= \left\{\sum_{i=1}^{4} e_i^2 + \frac{1}{2}\log\frac{k_h^2}{k_h^2 - e_5^2} \leq 2\rho_1\right\} \times \left\{\hat{D}_\gamma^2 + \hat{D}_q^2 \leq 2\rho_2\right\} \times \left\{h_r^2 + \dot{h}_r^2 + \ddot{h}_r^2 \leq \rho_3\right\}.
\end{aligned}
$$

Part I. To show that the filter error z_i is bounded in the compact set A_i.

Choose the Lyapunov function as

$$L_{z_i} = \frac{1}{2}z_i^2.$$

The virtual control law α_i will jump instantaneously at the time of switching instants t_σ, and without loss of generality, we assume that the filter error z_i satisfies

$$z_i\left(t_\sigma{}^+\right) = z_i\left(t_\sigma{}^-\right) + l_{z_i}^\sigma, \quad \sigma \in S, i = 2, 3, \cdots, 5.$$

Since the output of the filter is continuous, the magnitude of the $l_{z_i}^\sigma$ is completely determined by the difference of the adjacent switching modes. Consequently, the maximum of $l_{z_i}^\sigma$ can be expressed by

$$\max_\sigma \left| l^\sigma_{z_2} \right| = \max_\sigma \left| \alpha_2 \left(t_\sigma{}^+ \right) - \alpha_2 \left(t_\sigma{}^- \right) \right|$$

$$\leq \max_{\sigma_1, \sigma_2} \left| \left[\left(k_1^{\sigma 1} - k_1^{\sigma 2} \right) e_1 \right] / V \right|,$$

$$\max_\sigma \left| l^\sigma_{z_3} \right| = \max_\sigma \left| \alpha_3 \left(t_\sigma{}^+ \right) - \alpha_3 \left(t_\sigma{}^- \right) \right|$$

$$\leq \max_{\sigma_1, \sigma_2} \left| \left(k_2^{\sigma 1} - k_2^{\sigma 2} \right) e_2 + \left(f_\gamma^{\sigma 1} - f_\gamma^{\sigma 2} \right) \right| / \min_\sigma \left| g_\gamma^\sigma \right|,$$

$$\max_\sigma \left| l^\sigma_{z_4} \right| = \max_\sigma \left| \alpha_4 \left(t_\sigma{}^+ \right) - \alpha_4 \left(t_\sigma{}^- \right) \right|$$

$$\leq \max_{\sigma_1, \sigma_2} \left| \left(k_3^{\sigma 1} - k_3^{\sigma 2} \right) e_3 \right|,$$

$$\max_\sigma \left| l^\sigma_{z_5} \right| = \max_\sigma \left| \alpha_5 \left(t_\sigma{}^+ \right) - \alpha_5 \left(t_\sigma{}^- \right) \right|$$

$$\leq \max_{\sigma_1, \sigma_2} \left| \left(k_4^{\sigma 1} - k_4^{\sigma 2} \right) e_4 + \left(f_q^{\sigma 1} - f_q^{\sigma 2} \right) \right| / \min_\sigma \left| g_q^\sigma \right|.$$

Let $k_i^{\sigma 1} - k_i^{\sigma 2} \leq \bar{k}_{ci}, i = 1, 2, \cdots 5, \sigma_1, \sigma_2 \in S$. Then, in the case of $i = 2$, $\left| l^\sigma_{z_i} \right|$ have maximums on A, say M_{pz_2}. In the case of $i > 2$, $\left| l^\sigma_{z_i} \right|$ have maximums on $A \times A_{z_2} \times \cdots \times A_{z_{i-1}}, i > 2$, say M_{pzi}. The jumping of the Lyapunov function therefore can be given by

$$L_{zi} \left(t_\sigma{}^+ \right) - L_{zi} \left(t_\sigma{}^- \right) = l^{\sigma 2}_{zi} + 2 z_i \left(t_\sigma{}^- \right) l^\sigma_{zi}$$

$$\leq M^2_{pzi} + 2 \left| z_i \right| M_{pzi}.$$

Define the compact set $A_{zi} = \{ z_i^2 \leq M_{pli} \}$, where $M_{pli} > \left(1 + \sqrt{2} \right)^2 M^2_{pzi}$, so that the jumping of the Lyapunov function have maximum $M^2_{pzi} + 2\sqrt{M_{pli}} M_{pzi}$ on the compact set $A \times A_{z_2} \times \cdots \times A_{z_i}$. For every interval between two consecutive switching times $t \in \left[t_\sigma{}^+, t_{\sigma+1}{}^- \right)$,

$$\dot{L}_{zi} = -\frac{1}{\tau_i} z_i^2 - z_i \dot{\alpha}^\sigma_{i-1}. \tag{24}$$

There exist continuous functions η_{dz_i} such that

$$\left| \dot{\alpha}^\sigma_1 \right| \leq \eta_{dz_2} \left(e_1, e_2, z_2, k_1, h_r, \dot{h}_r, \ddot{h}_r, V, \dot{V} \right),$$

$$\left| \dot{\alpha}^\sigma_2 \right| \leq \eta_{dz_3} \left(e_1, e_2, e_3, z_2, z_3, k_1, k_2, \hat{D}_\gamma, h_r, \dot{h}_r, \ddot{h}_r, V, \dot{V} \right),$$

$$\left| \dot{\alpha}^\sigma_3 \right| \leq \eta_{dz_4} \left(e_1, e_2, e_3, e_4, z_2, z_3, z_4, k_1, k_2, k_3, \hat{D}_\gamma, h_r, \dot{h}_r, \ddot{h}_r, V, \dot{V} \right),$$

$$\left| \dot{\alpha}^\sigma_4 \right| \leq \eta_{dz_5} \left(e_1, e_2, e_3, e_4, e_5, z_2, z_3, z_4, z_5, k_1, k_2, k_3, k_4, \hat{D}_\gamma, \hat{D}_q, h_r, \dot{h}_r, \ddot{h}_r, V, \dot{V} \right),$$

and η_{dz_i} have maximums on the compact set $A \times A_{z2} \times \cdots \times A_{zi}$, say M^σ_{zi}. Define $M_{zi} = \max_\sigma M^\sigma_{zi}$, according to Young's inequality, it holds that

$$z_i \dot{\alpha}_{i-1} \leq \frac{(M_{zi} z_i)^2}{2 \varepsilon_{zi}} + \varepsilon_{zi}. \tag{25}$$

Substituting Eq. (25) into (24) yields

$$\dot{L}_{zi} \leq -\left(\frac{1}{\tau_i} - \frac{M_{zi}^2}{2 \varepsilon_{zi}} \right) z_i^2 + \varepsilon_{zi}.$$

Let $\frac{1}{\tau_i} = \frac{M_{d\gamma}^2}{2 \varepsilon_\gamma} + a_{i0}$, then $\dot{L}_{zi} \leq -2 a_{i0} L_{zi} + \varepsilon_{zi}$ for $t \in \left[t_\sigma{}^+, t_{\sigma+1}{}^- \right)$. Define $L_{mz_i} = L_{zi} - \frac{\varepsilon_{zi}}{2 a_{i0}}$, then $\dot{L}_{mz_i} \leq -2 a_0 L_{mz_i}$. for $t \in \left[t_\sigma{}^+, t_{\sigma+1}{}^- \right)$, we have

$$L_{mz_i} (t) \leq L_{mz_i} \left(t_\sigma^+ \right) e^{-2 a_0 (t - t_\sigma)}.$$

Let

$$\Delta M_i = M_{pli} - M^2_{pzi} - 2\sqrt{M_{pli}} M_{pzi}$$

$$= \Delta m_{i1} + \Delta m_{i2}, \tag{26}$$

L_{mz_i} will decrease on each time interval $t \in \left[t_\sigma{}^+, t_{\sigma+1}{}^- \right)$, and therefore, the maximum of L_{mz_i}, say M_{lmi} will appear at $t_\sigma{}^+$ and satisfy the following inequality

$$M_{lmi} \left(1 - e^{-2 a_0 \mu_m} \right) \geq M^2_{pzi} + 2\sqrt{M_{pli}} M_{pzi},$$

such that the minimum decreased value is no less than the maximum jumping. Therefore, L_{mz_i} has maximum $M_{lmi} = \frac{M^2_{pzi} + 2\sqrt{M_{pli}} M_{pzi}}{(1 - e^{-2 a_0 \mu_m})}$. In order to guarantee that the magnitude of M_{lmi} cannot exceed the compact set A_{zi}, let

$$\frac{M_{pzi}^2 + 2\sqrt{M_{pli}}M_{pzi}}{\left(1 - e^{-2a_0\mu_m}\right)} \leq M_{pli} - \Delta m_{i1}$$

and

$$
\begin{aligned}
\Delta M_i &= M_{pli} - M_{pzi}^2 - 2\sqrt{M_{pli}}M_{pzi} \\
&= \Delta m_{i1} + \Delta m_{i2},
\end{aligned}
\tag{27}
$$

in which Δm_1 and $\Delta m_2 > 0$. Combining Eq. (26) with (27) results in

$$a_{i0} \geq \frac{1}{2\mu_m} \ln \frac{M_{pli} - \Delta m_{i1}}{\Delta m_{i2}}.$$

According to $L_{zi} = L_{mzi} + \frac{\varepsilon_{zi}}{2a_{i0}}$, it holds that $L_{zi} \leq M_{pli} - \Delta m_{i1} + \frac{\varepsilon_{zi}}{2a_{i0}}$.

Let $a_{i0} \geq \max\left\{\frac{\varepsilon_{zi}}{2\Delta m_1}, \frac{1}{2\mu_m} \ln \frac{M_{pli} - \Delta m_{i1}}{\Delta m_{i2}}\right\}$, then, z_i will remain in the compact set A_{zi}. The process of Part I can be recursive from $i = 2$ to $i = 5$, and define $A_z = A_{z2} \times A_{z3} \times A_{z4} \times A_{z5}$.

Part II. To show A is an invariant set.

Note that there exist continuous functions $\eta_{d\gamma}$, η_{dq} such that

$$
\begin{aligned}
\max_\sigma D_\gamma &\leq \eta_{d\gamma}\left(h_r, \dot{h}_r, e_1, e_2, e_3, z_1, \underset{\sigma=1,2,\cdots l}{k_1^\sigma}, V\right), \\
\max_\sigma D_q &\leq \eta_{dq}\left(h_r, \dot{h}_r, e_1, e_2, e_3, e_4, z_1, z_2, z_3, \underset{\sigma=1,2,\cdots l}{k_2^\sigma}, \underset{\sigma=1,2,\cdots l}{k_3^\sigma}, V\right).
\end{aligned}
$$

It is not hard to verify $\eta_{d\gamma}$ and η_{dq} have maximums on $A \times A_z$, say $\bar{D}_\gamma$ and $\bar{D}_q$ respectively. We define $\tilde{D}_\gamma = D_\gamma - \bar{D}_\gamma$, $\tilde{D}_q = D_q - \bar{D}_q$. Choose the candidate Lyapunov function as

$$L_D = \frac{1}{2}\hat{D}_\gamma^2 + \frac{1}{2}\hat{D}_q^2. \tag{28}$$

Take the derivative of Eq. (28) gives

$$\dot{L}_D = -k_{d\gamma}\hat{D}_\gamma^2 - k_{dq}\hat{D}_q^2 + \hat{D}_\gamma |e_2| + \hat{D}_q |e_4|.$$

Be aware of that $|e_2|$ and $|e_4|$ have maximum of $\sqrt{2\rho_1}$ on the compact set A, thus we have that

$$\dot{L}_D \leq -\left(k_{d\gamma} - \frac{\rho_1}{\varepsilon_{de\gamma}}\right)\hat{D}_\gamma^2 - \left(k_{dq} - \frac{\rho_1}{\varepsilon_{deq}}\right)\hat{D}_q^2 + \varepsilon_{de\gamma} + \varepsilon_{deq}.$$

Let $k_{d\gamma} = a_D + \frac{\rho_1}{\varepsilon_{de\gamma}}$ and $k_{dq} = a_D + \frac{\rho_1}{\varepsilon_{deq}}$, it follows that $\dot{L}_D \leq -2a_D L_D + b_D$. Let $a_D > \frac{b_D}{2\rho_2}$, then $\dot{L}_D < 0$ on $L_D = \rho_2$. Therefore, if e_1, e_2, e_2, e_3, and e_4 do not exceed the compact set A, then $\hat{D}_\gamma$, and $\hat{D}_q$ will remain in the compact set A. Combine Lemma 2 with the Lyapunov function of the tracking error as

$$
\begin{aligned}
\dot{L}_{h5} =\ & -k_1^\sigma e_1^2 - (1 - \lambda_\gamma)k_2^\sigma e_2^2 - k_3^\sigma e_3^2 - (1 - \lambda_q)k_4^\sigma e_4^2 + \frac{k_5 e_5^2}{k_{b_5}^2 - e_5^2} - g_q^\sigma e_4 e_5 \\
& + V e_1 z_2 + g_\gamma^\sigma e_2 z_3 + e_3 z_4 + g_q^\sigma e_4 z_5 + |e_2| D_\gamma^\sigma - \hat{D}_\gamma e_2 \tanh\left(\frac{c\hat{D}_\gamma e_2}{\varepsilon_V}\right) \\
& + \lambda_\gamma \left| e_2 \hat{D}_\gamma \tanh\left(\frac{c e_2 \hat{D}_\gamma}{\varepsilon_V}\right) \right| + |e_4| D_q^\sigma - \hat{D}_q e_4 \tanh\left(\frac{c\hat{D}_q e_4}{\varepsilon_V}\right) \\
& + \lambda_q \left| e_4 \hat{D}_q \tanh\left(\frac{c e_4 \hat{D}_q}{\varepsilon_V}\right) \right| \\
\leq\ & -k_1^\sigma e_1^2 - (1 - \lambda_\gamma)k_2^\sigma e_2^2 - k_3^\sigma e_3^2 - (1 - \lambda_q)k_4^\sigma e_4^2 + \frac{k_5 e_5^2}{k_{b_5}^2 - e_5^2} + V e_1 z_2 \\
& + g_\gamma^\sigma e_2 z_3 + e_3 z_4 + g_q^\sigma e_4 z_5 + + |e_2|\left[(1 - \lambda_\gamma)\tilde{D}_\gamma + \lambda_\gamma \bar{D}_\gamma\right] \\
& + |e_4|\left[(1 - \lambda_q)\tilde{D}_q + \lambda_q \bar{D}_q\right].
\end{aligned}
$$

There is a maximum value of $(1 - \lambda_\gamma)\tilde{D}_\gamma + \lambda_\gamma \bar{D}_\gamma$ on the compact set $A \times A_z$, independent of k_1^σ, denoted by $M_{D\gamma}$. And there is a maximum value of $(1 - \lambda_q)\tilde{D}_q + \lambda_q \bar{D}_q$ independent of k_4^σ, denoted as M_{Dq}. According to Young's inequality, the following inequalities hold:

$$|e_2|\left[(1-\lambda_\gamma)\tilde{D}_\gamma + \lambda_\gamma \bar{D}_\gamma\right] \le \frac{M_{D\gamma}^2 e_2^2}{2\varepsilon_{D\gamma}} + \varepsilon_{D\gamma},$$

$$|e_4|\left[(1-\lambda_q)\tilde{D}_q + \lambda_q \bar{D}_q\right] \le \frac{M_{Dq}^2 e_4^2}{2\varepsilon_{Dq}} + \varepsilon_{Dq},$$

$$Ve_1 z_2 \le \frac{V^2 z_2^2}{4\lambda_1} + \lambda_1 e_1^2 \le M_{\lambda_1} z_2^2 + \lambda_1 e_1^2,$$

$$g_\gamma^\sigma e_2 z_3 \le \frac{g_\gamma^{\sigma 2} z_3^2}{4\lambda_2} + \lambda_2 e_2^2 \le M_{\lambda_2} z_3^2 + \lambda_2 e_2^2, \qquad (29)$$

$$e_3 z_4 \le \frac{z_4^2}{4\lambda_3} + \lambda_3 e_3^2 \le M_{\lambda_3} z_4^2 + \lambda_3 e_3^2,$$

$$g_q^\sigma e_4 z_5 \le \frac{g_q^{\sigma 2} z_5^2}{4\lambda_4} + \lambda_4 e_4^2 \le M_{\lambda_4} z_5^2 + \lambda_4 e_4^2,$$

where M_{λ_1}, M_{λ_2}, M_{λ_3}, M_{λ_4} are the maximum magnitude of $\frac{V^2}{4\lambda_1}$, $\frac{\left(g_\gamma^\sigma\right)^2}{4\lambda_2}$, $\frac{1}{4\lambda_3}$, $g_q^\sigma e_4 z_5 \le \frac{\left(g_q^\sigma\right)^2}{4\lambda_4} + \lambda_4 e_4^2$, respectively. Therefore, for $t \in [t_\sigma^+, t_{\sigma+1}^-)$, one has

$$\dot{L}_{h5} \le -\left(k_1^\sigma - \lambda_1\right)e_1^2 - \left[(1-\lambda_\gamma)k_2^\sigma - \lambda_2 - \frac{M_{D\gamma}^2}{2\varepsilon_{D\gamma}}\right]e_2^2 - \left(k_3^\sigma - \lambda_3\right)e_3^2$$

$$- \left[(1-\lambda_q)k_4^\sigma - \lambda_4 - \frac{M_{Dq}^2}{2\varepsilon_{Dq}}\right]e_4^2 + \frac{k_5 e_5^2}{k_{b_5}^2 - e_5^2} + b_h,$$

where $b_h = \varepsilon_{D\gamma} + \varepsilon_{Dq} + \sum_{i=1}^{6} M_{\lambda_i} M_{pli}$, let $k_1^\sigma = \lambda_1 + \alpha_h^\sigma$, $k_2^\sigma = \frac{\lambda_2 + \alpha_h^\sigma + \frac{M_{D\gamma}^2}{2\varepsilon_{D\gamma}}}{1-\lambda_\gamma}$, $k_3^\sigma = \lambda_3 + \alpha_h^\sigma$, and $k_4^\sigma = \frac{\lambda_4 + \alpha_h^\sigma + \frac{M_{Dq}^2}{2\varepsilon_{Dq}}}{1-\lambda_q}$, it holds that $\dot{L}_{h5} \le -2a_h^\sigma L_{h5} + b_h$. Let $\min_\sigma a_h^\sigma > \frac{nb_h}{2\rho_1}, n \ge 1$, it holds that $\dot{L}_{h5} < 0$ on $L_{h5} = \rho_1$. As a consequence, it can be concluded that the compact set A is an invariant set.

Part III. To show the convergence of the tracking error.

For each interval $t \in [t_\sigma^+, t_{\sigma+1}^-)$, it holds that

$$L_{h5}(t) \le \left(L_{h5}(t_\sigma^-) - \frac{b_h}{a_h^\sigma}\right)e^{-a_h^\sigma(t-t_\sigma)} + \frac{b_h}{a_h^\sigma}$$

$$\le L_{h5}(t_\sigma^-)e^{-a_h^\sigma(t-t_\sigma)} + \frac{b_h}{\underline{a}_h}\left(1 - e^{-a_h^\sigma(t-t_\sigma)}\right) \qquad (30)$$

$$= \left(L_{h5}(t_\sigma^-) - \frac{b_h}{\underline{a}_h}\right)e^{-a_h^\sigma(t-t_\sigma)} + \frac{b_h}{\underline{a}_h},$$

where $\underline{a}_h = \min_\sigma a_h^\sigma$. $\square$

Remark 6. The virtual control law α_i is not differentiable at the moment of switching instant, hence Eq. (30) can only hold in every interval between the two consecutive switching times.

Let $L_{mh} = L_{h5} - \frac{b_h}{\underline{a}_h}$, then $L_{mh}(t) \le L_{mh}(t_\sigma^+)e^{-a_h^\sigma(t-t_\sigma)}$, we can verify that $L_{mh}(t_\sigma^+) = L_{mh}(t_\sigma^-)$. Therefore, $\lim_{t \to \infty} L_{mh}(t) \le 0$, and it follows that

$$\lim_{t \to \infty} e_1 \le \sqrt{\frac{2b_h}{\underline{a}_h}}.$$

Since b_h is independent of k_1^σ, k_2^σ, k_3^σ and k_4^σ, if $\underline{a}_h$ is large enough, e_1 can be arbitrarily small. Therefore, it can be verified that the conditions of Lemma 3 are satisfied on every interval between the two consecutive switching instants, so that $|e_5|$ will not exceed k_h.

Remark 7. Since $e_5 = \delta_a - \alpha_{4c}$, and α_{4c} can be arbitrary, and thus, the condition $|e_5(0)| < k_h$ in Theorem 1 can always be satisfied. Furthermore, the velocity usually changes slower than the altitude angle, and thus, V and $\dot{V}$ are regarded as bounded variables in the proof of Theorem 1, which is a weak assumption generally used in the existing literature.

3.4. Velocity controller design

Define the tracking error as $e_{v1} = V - V_r$, $e_{v2} = T_e - \alpha_{vc}$, where α_{vc} is the output of the first-order filter with the virtual control law as the input, which is given below as

$$\dot{\alpha}_{vc} = \frac{1}{\tau_v}\left(\alpha_v^\sigma - \alpha_{vc}\right), \alpha_{vc}\left(0\right) = \alpha_v^\sigma\left(0\right). \tag{31}$$

Step 1: Define the Lyapunov function as $L_{V_1} = \frac{1}{2}e_{v1}^2$, taking the derivative of L_{V_1} yields

$$\dot{L}_{v1} = e_{v_1}\left[f_v^\sigma + g_v\left(\alpha_v^\sigma + e_v + z_v\right) + \Delta_v^\sigma + d_v - \dot{V}_r\right], \tag{32}$$

where $\Delta_v^\sigma = f_v^\sigma - f_v$. Design the virtual control law as

$$\alpha_v^\sigma = \frac{1}{g_v}\left[-k_v^\sigma e_{v1} + \dot{V}_r - f_v^\sigma - \hat{D}_v \tanh\left(\frac{ce_{v1}\hat{D}_v}{\varepsilon_V}\right)\right], \tag{33}$$

where $\hat{D}_v$ is adapted by

$$\dot{\hat{D}}_v = |e_{v1}| - k_{Dv}\hat{D}_\gamma. \tag{34}$$

Substituting (33), (34) into (32) yields

$$\dot{L}_{v1} = -k_v^\sigma e_{v1}^2 + e_v\left(d_v + \Delta_v\right) + g_v e_{v1}\left(z_v + e_{v2}\right) - \hat{D}_v e_{v1}\tanh\left(\frac{c\hat{D}_v e_{v1}}{\varepsilon_V}\right),$$

where $D_v^\sigma = \left|d_v + \Delta_v^\sigma\right|$.

Step 2: Choose the Lyapunov function as

$$L_{v2} = L_{v1} + \frac{1}{2}\log\frac{k_v^2}{k_v^2 - e_{v2}^2}. \tag{35}$$

Taking the derivative of Eq. (35) leads to

$$\dot{L}_{v2} = \dot{L}_{v1} + \frac{e_{v2}}{k_v^2 - e_{v2}^2}\left[\frac{1}{T_{te}}\left(T_{cm} - T_e\right) - \dot{\alpha}_{vc}\right]. \tag{36}$$

Design the control law as

$$T_{cm}^\sigma = T_e + T_{te}\left[-k_{v2}e_{v2} + \dot{a}_{cv} - (k_v^2 - e_{v2}^2)g_v e_{v1}\right]. \tag{37}$$

Then, we have

$$\dot{L}_{v2} = \dot{L}_{v1} + \frac{k_{v2}^2 e_{v2}^2}{k_v^2 - e_{v2}^2} - g_v^\sigma e_{v1}e_{v2}.$$

Theorem 2. *Consider the closed-loop system composed by (10), by the control laws (33), (37), and the adaptive laws (34). Let Assumptions 1, 3, 4, 5, 6 hold. Given any initial error condition $|e_{v2}(0)| < k_v$, there exist a set of design parameters, such that all the signals of the closed-loop system remain bounded, and the velocity tracking error e_{v1} will converge to a small neighborhood of the origin determined by the design parameters. Furthermore, e_{v2} will remain in the set $|e_{v2}| < k_v$.*

Proof. The proof of Theorem 2 is analogous to that of Theorem 1, and thus, we omit it here owing to space limitations. □

4. Simulation

We present a comparison simulation to demonstrate the control performance of our proposed control scheme. The controller proposed in this paper is compared with the method proposed in [26], which gives the design of the controllers based on the nonlinear morphing aircraft model with fixed altitude and Mach number. To illustrate the effectiveness of the proposed controllers, the cases devoid of switching and actuator dynamics are also simulated. For the sake of brevity, the method proposed in this paper is represented by m_1, and the switching controller without considering the actuator dynamics is represented by m_2. Further, the non-switching controller method is represented by m_3, and the method in [26] is represented by m_4.

To satisfy Assumption 4, the reference signals h_r and V_r have been obtained from the square waves passing through the second-order filter $H_r(s) = \frac{0.00144}{s^2 + 0.077s + 0.00144}$. The sweep angle signal is obtained from the square wave passed through the second-order filter $H_s(s) = \frac{0.0064}{s^2 + 0.08s + 0.0064}$, which makes the signal change smooth. Fig. 5 depicts the mission profile of a morphing aircraft which climbs from a high lift configuration to a maneuver configuration, and then back to the high lift configuration.

In the simulation described in this paper, actuator parameters are set as $T_\delta = 0.05$ and $T_T = 0.2$. The initial conditions are set as $[h_0, \gamma_0, \theta_0, q_0, V_0, \delta_{e0}, T_0] = [1500\text{ m}, 0°, 1.72°, 0°/s, 140\text{ m/s}, -1.08°, 5600\text{ N}]$. Filter parameters are selected as, viz., $\tau_1 = 0.01$, $\tau_2 = 0.01$, $\tau_3 = 0.01$, $\tau_4 = 0.02$, and $\tau_v = 0.1$. Tracking error limits are set as $k_{b1} = 0.6$ and $k_{b2} = 0.2$. Gains for adaptive laws are selected as $k_{D1} = 1$, $k_{D2} = 1$, and $k_{Dv} = 2$. Gains for the switching controllers are listed in Table 1, and gains for non-switching controller of m_3 are selected as $k_1 = 2$, $k_2 = 7.8$, $k_3 = 3$, $k_4 = 5.4$, $k_5 = 1$, $k_{v1} = 2.5$, and $k_{v2} = 3$.

The results from the simulation are shown in Figs. 6-13. Figs. 6-8 reveal the tracking errors and the root mean square errors (RSME) $\left[\frac{1}{T}\int_0^t e^2 dt\right]^{\frac{1}{2}}$ of altitude and velocity subsystems, when the morphing does not occur during $t \in [0s, 20s]$, the tracking errors of all the four methods have negligible difference. However, with the occurrence of morphing and the changes of the altitude and Mach number,
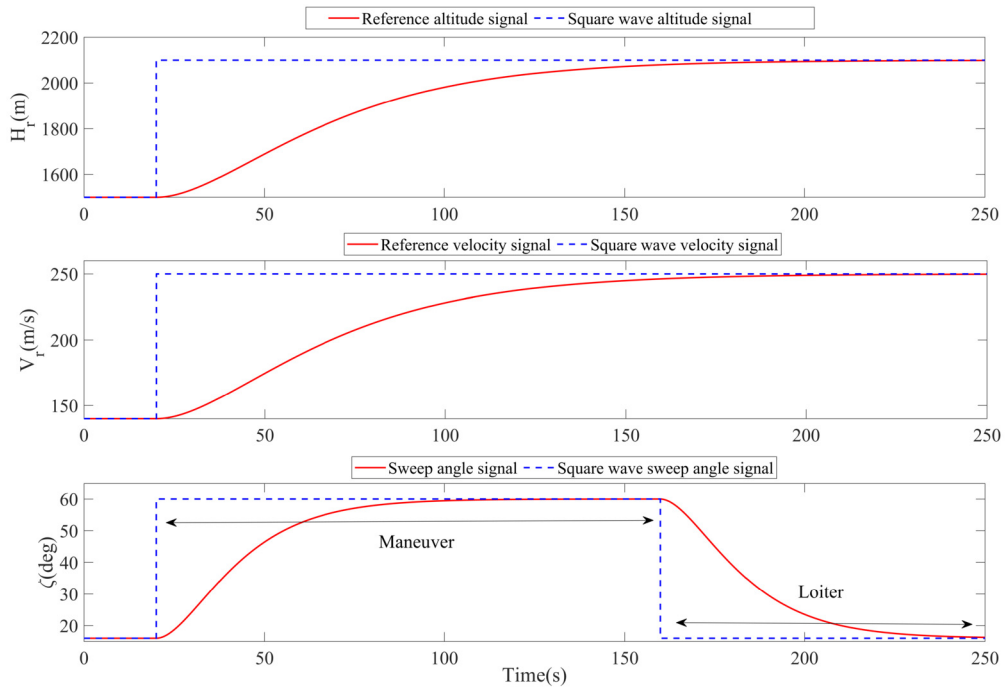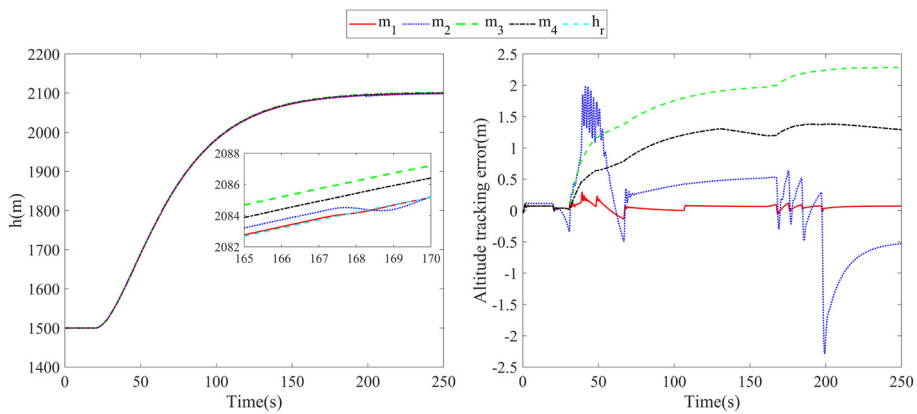
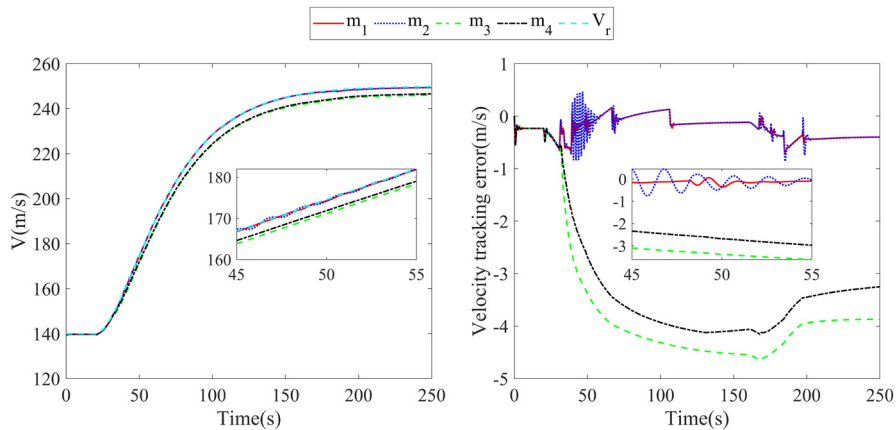**Fig. 5.** Reference signals and sweep angle change law.

Fig. 6. Altitude tracking.

Fig. 7. Velocity tracking.
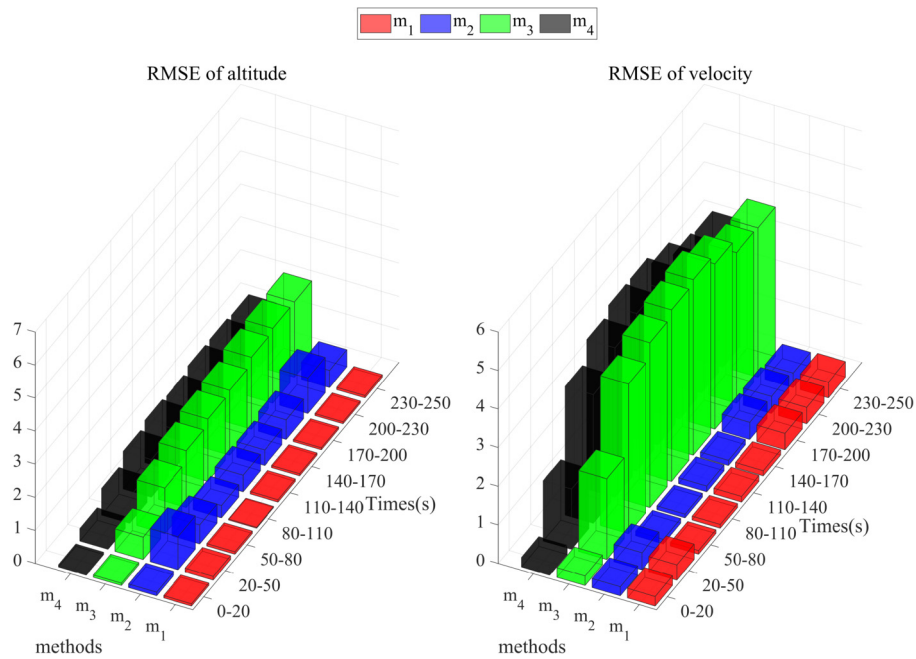
Fig. 8. RSME for different methods.
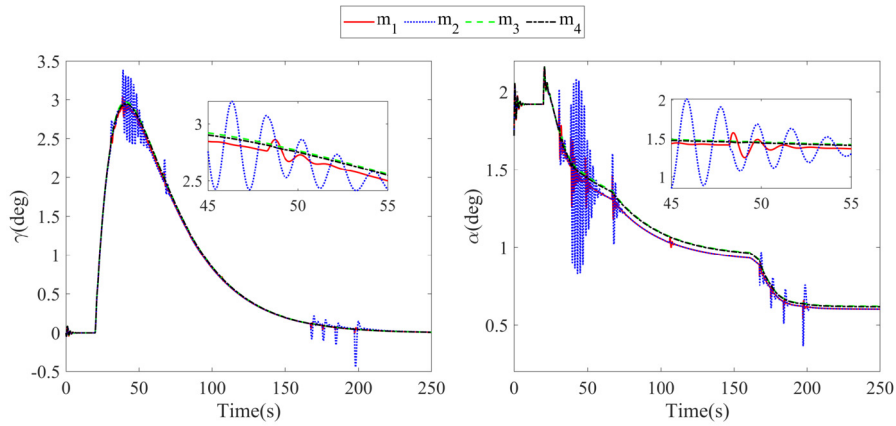
Fig. 9. The responses of γ and α.
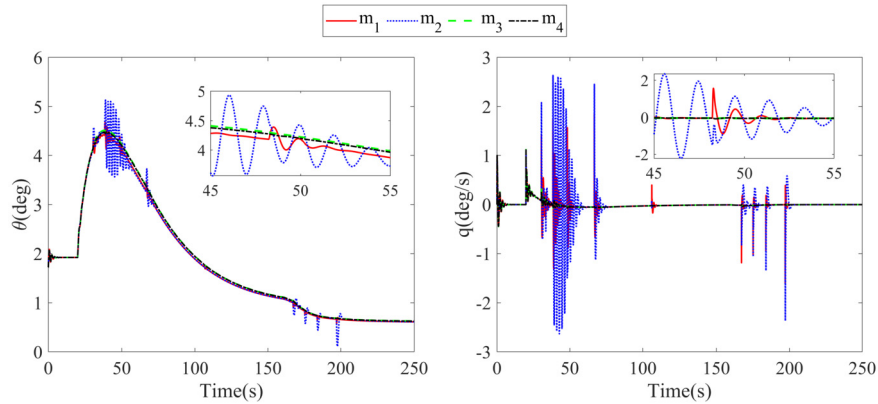
Fig. 10. The responses of θ and q.

Table 1
Gains for the switching controllers.

Modes	Gains for the different modes						
	k_1	k_2	k_3	k_4	k_5	k_{v1}	k_{v2}
$\sigma = 21$	2	8	3	7	1	2	3
$\sigma = 22$	2	7.6	3	6.6	1	2	3
$\sigma = 23$	2	7.2	3	6.3	1	2.5	3
$\sigma = 28$	2	7.0	3	5.5	1	2.5	3
$\sigma = 29$	2	7.6	2.8	5.2	1	3	3
$\sigma = 30$	2	7.6	2.4	4.5	1	3.5	3
$\sigma = 45$	2	8	2	4.5	1	3.5	3
$\sigma = 44$	2	7.6	1.6	4.1	1	3	3
$\sigma = 43$	2	7.2	2.7	4.8	1	2.5	3
$\sigma = 42$	2	7	3.3	5.8	1	2.5	3
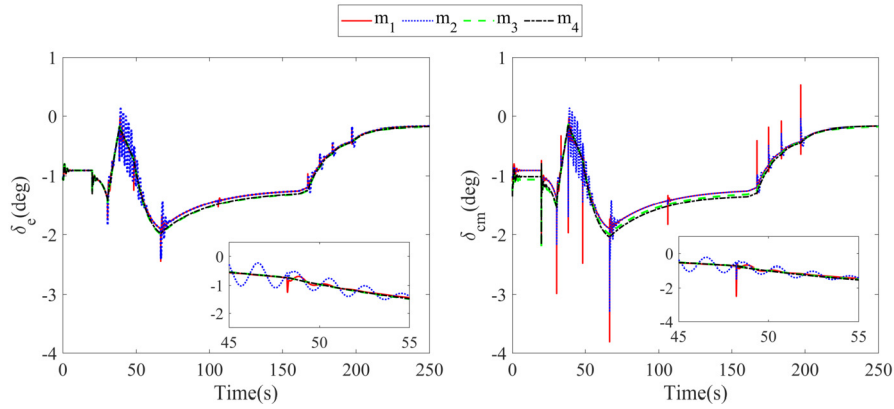
Fig. 11. The control inputs δ_e and δ_{cm}.
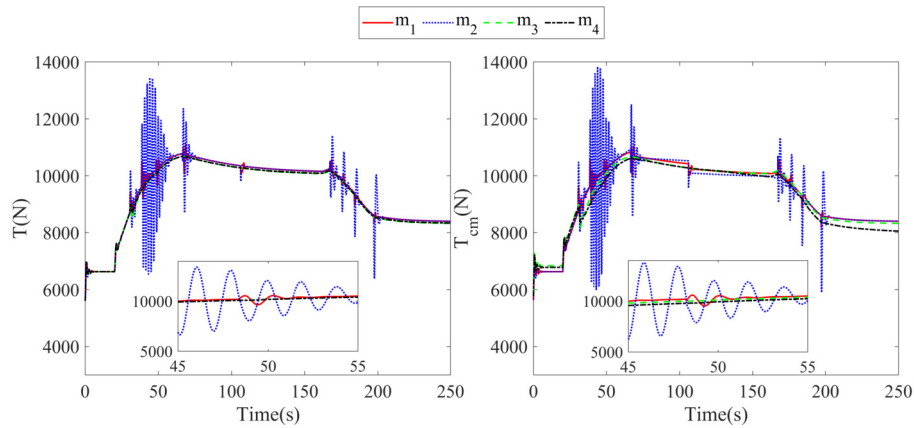

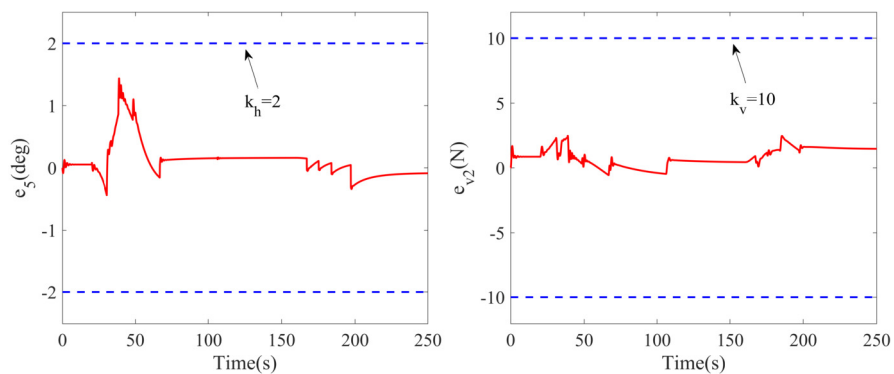**Fig. 12.** The control inputs T and T_{cm}.

Fig. 13. The tracking errors of actuators of m_1.

the tracking performance of m_1 excels other methods. m_2 has better tracking performance than m_3 and m_4 in most time periods owing to the taking of all the changes of the model parameters into account, and designing different control laws for various flight conditions. Nevertheless, during $t \in [20\,s, 50\,s]$ and $t \in [200\,s, 230\,s]$, the occurrence of the chatter leads to larger altitude tracking error. m_4 has better tracking performance than m_3 owing to the employment of neural network to estimate the uncertainty caused by the morphing, though the improvement brought by this estimation is limited. The responses of the state variables of the closed-loop system are depicted in Figs. 9-10. Accordingly, α, γ, θ, q stay bounded and eventually reach a new equilibrium point. Figs. 11-12 show the command signals of actuators. According to Figs. 9-12, the switching of the control laws may cause chattering phenomenon, and the comparison between m_1 and m_2 demonstrates that this problem can be alleviated by including the actuator dynamics in the controller design process. Fig. 13 illustrates the dynamics and the tracking errors of the actuators. Owing to the introduction of the barrier Lyapunov function technique, the tracking errors e_5 and e_{v2} are always limited in the preset range, which improves the tracking performance of the closed-loop system.

5. Conclusion

The modeling and control of the morphing aircraft have been explored in this study. A nonlinear morphing aircraft model suitable for larger envelopes is first demonstrated, which elaborates the variation of the aerodynamic coefficients and mass distribution at different altitudes, Mach numbers, and sweep angles. We employ a continuous nonlinear model combined with a switching controller to replace the switching morphing aircraft model, which describes the dynamic characteristics of the aircraft more accurately than switching model. Concomitantly, the switching of the control laws makes it challenging to perform the stability analysis. To solve this problem, we quantify the jumping of Lyapunov functions by introducing the concept of a compact set, and prove the stability of the closed-loop system. Furthermore, this article includes the actuator dynamics in the controller design process, and introduces the Lyapunov barrier function to improve the dynamic response of the actuators, which alleviates the chatter phenomenon caused by the switching. Finally, the results from the simulation verify the effectiveness of the proposed method in this paper.

We will focus on designing a smoother switching nonlinear controller, in a future work, to improve the performance of the transition process of the switching, and we will apply that to the six degrees of freedom of the morphing aircraft model.

Declaration of competing interest

The authors declare that they have no known competing financial interests or personal relationships that could have appeared to influence the work reported in this paper.

Acknowledgements

References

[1] M. Nemati, A. Jahangirian, Robust aerodynamic morphing shape optimization for high-lift missions, Aerosp. Sci. Technol. 103 (2020) 105897.

[2] R.M. Ajaj, C.S. Beaverstock, M.I. Friswell, Morphing aircraft: The need for a new design philosophy, Aerosp. Sci. Technol. 49 (2016) 154–166.

[3] D.C. Li, S.W. Zhao, A. Da Ronch, J.W. Xiang, J. Drofelnik, Y.C. Li, L. Zhang, Y.N. Wu, M. Kintscher, H.P. Monner, A. Rudenko, S.J. Guo, W.L. Yin, J. Kirn, S. Storm, R. De Breuker, A review of modelling and analysis of morphing wings, Prog. Aerosp. Sci. 100 (2018) 46–62.

[4] E. Lamacchia, A. Pirrera, I.V. Chenchiah, P.M. Weaver, Morphing shell structures: a generalised modelling approach, Compos. Struct. 131 (2015) 1017–1027.

[5] F. Nicassio, Shape prediction of bistable plates based on Timoshenko and Ashwell theories, Compos. Struct. 265 (2021) 113645.

[6] S. Barbarino, E.I. Saavedra Flores, R.M. Ajaj, I. Dayyani, M.I. Friswell, A review on shape memory alloys with applications to morphing aircraft, Smart Mater. Struct. 23 (6) (2014) 063001.

[7] P. Dai, B. Yan, W. Huang, Y. Zhen, M. Wang, S. Liu, Design and aerodynamic performance analysis of a variable-sweep-wing morphing waverider, Aerosp. Sci. Technol. 98 (2020) 105703.

[8] Z. Hui, Y. Zhang, G. Chen, Aerodynamic performance investigation on a morphing unmanned aerial vehicle with bio-inspired discrete wing structures, Aerosp. Sci. Technol. 95 (2019) 105419.

[9] A. Quintana, G. Graves, M. Hassanalian, A. Abdelkefi, Aerodynamic analysis and structural integrity for optimal performance of sweeping and spanning morphing unmanned air vehicles, Aerosp. Sci. Technol. 110 (2021) 106458.

[10] A. Roy, R. Mukherjee, Three dimensional rectangular wing morphed to prevent stall and operate at design local two dimensional lift coefficient, Aerosp. Sci. Technol. 107 (2020) 106312.

[11] M. Leonard, T. Ilhan, Integrated approach to the dynamics and control of maneuvering flexible aircraft, Report NASA/CR-2003-211748, 2003.

[12] M. Mohamed, G. Madhavan, Reduced order model based flight control system for a flexible aircraft, in: 6th Conference on Advances in Control and Optimization of Dynamical Systems (ACODS), vol. 53, 2020, pp. 75–80.

[13] B.B. Yan, Y. Li, P. Dai, S.X. Liu, Aerodynamic analysis, dynamic modeling, and control of a morphing aircraft, J. Aerosp. Eng. 32 (2019) 04019058.

[14] N. Wen, Z.H. Liu, Y. Sun, L.P. Zhu, Design of LPV-based sliding mode controller with finite time convergence for a morphing aircraft, Int. J. Aerosp. Eng. 2018 (2018) 1–20.

[15] N. Wen, Z. Liu, L. Zhu, Linear-parameter-varying-based adaptive sliding mode control with bounded L_2 gain performance for a morphing aircraft, Proc. Inst. Mech. Eng. 233 (5) (2019) 1847–1864.

[16] Q. Wu, Z.H. Liu, F.N. Liu, X.K. Chen, LPV-based self-adaption integral sliding mode controller with L_2 gain performance for a morphing aircraft, IEEE Access 7 (2019) 81515–81531.

[17] D.H. Baldelli, D.H. Lee, R.S.S. Pena, B. Cannon, Modeling and control of an aeroelastic morphing vehicle, J. Guid. Control Dyn. 31 (6) (2008) 1687–1699.

[18] Z. He, M. Yin, Y.P. Lu, Tensor product model-based control of morphing aircraft in transition process, Proc. Inst. Mech. Eng., G J. Aerosp. Eng. 230 (2) (2016) 378–391.

[19] X.M. Wang, W.Y. Zhou, R.N. Mu, Z.G. Wu, A new deformation control approach for flexible wings using moving masses, Aerosp. Sci. Technol. 106 (2020) 106118.

[20] W.L. Jiang, C.Y. Dong, Q. Wang, A systematic method of smooth switching LPV controllers design for a morphing aircraft, Chin. J. Aeronaut. 28 (6) (2015) 1640–1649.

[21] H.Y. Cheng, C.Y. Dong, W.L. Jiang, Q. Wang, Y.Z. Hou, Non-fragile switched h-infinity control for morphing aircraft with asynchronous switching, Chin. J. Aeronaut. 30 (3) (2017) 1127–1139.

[22] W. Jiang, K. Wu, Z. Wang, Y. Wang, Gain-scheduled control for morphing aircraft via switching polytopic linear parameter-varying systems, Aerosp. Sci. Technol. 107 (2020) 106242.

[23] J. Lee, Y. Kim, Neural network-based nonlinear dynamic inversion control of variable-span morphing aircraft, Proc. Inst. Mech. Eng., G J. Aerosp. Eng. 234 (10) (2020) 1624–1637.

[24] T. Yue, X. Zhang, L. Wang, J. Ai, Flight dynamic modeling and control for a telescopic wing morphing aircraft via asymmetric wing morphing, Aerosp. Sci. Technol. 70 (2017) 328–338.

[25] B. Yan, P. Dai, R. Liu, M. Xing, S. Liu, Adaptive super-twisting sliding mode control of variable sweep morphing aircraft, Aerosp. Sci. Technol. 92 (2019) 198–210.

[26] Z.H. Wu, J.C. Lu, Q. Zhou, J.P. Shi, Modified adaptive neural dynamic surface control for morphing aircraft with input and output constraints, Nonlinear Dyn. 87 (4) (2017) 2367–2383.

[27] Z.H. Wu, J.C. Lu, J.P. Shi, Y. Liu, Q. Zhou, Robust adaptive neural control of morphing aircraft with prescribed performance, Math. Probl. Eng. 2017 (2017) 1–16.

[28] L.G. Gong, Q. Wang, C.Y. Dong, Disturbance rejection control of morphing aircraft based on switched nonlinear systems, Nonlinear Dyn. 96 (2) (2019) 975–995.

[29] Q. Wang, L. Gong, C. Dong, K. Zhong, Morphing aircraft control based on switched nonlinear systems and adaptive dynamic programming, Aerosp. Sci. Technol. 93 (2019) 105325.

[30] P.Y. Shao, J. Wu, C.F. Wu, S.H. Ma, Model and robust gain-scheduled PID control of a bio-inspired morphing UAV based on LPV method, Asian J. Control 21 (4) (2019) 1681–1705.

[31] M. Lv, D. Schutter, C. Shi, S. Baldi, Logic-based distributed switching control for agents in power chained form with multiple unknown control directions, Automatica 137 (2022) 110143.

[32] M. Lv, W. Yu, J. Cao, S. Baldi, A separation-based methodology to consensus tracking of switched high-order nonlinear multiagent systems, IEEE Trans. Neural Netw. Learn. Syst. (2021) 1–13.

[33] Z.P. Yan, Z.W. Yang, J.Z. Zhang, J.J. Zhou, A.Z. Jiang, X. Du, Trajectory tracking control of UUV based on backstepping sliding mode with fuzzy switching gain in diving plane, IEEE Access 7 (2019) 166788–166795.

[34] D. Swaroop, J.K. Hedrick, P.P. Yip, J.C. Gerdes, Dynamic surface control for a class of nonlinear systems, IEEE Trans. Autom. Control 45 (10) (2000) 1893–1899.

[35] T. Seigler, Dynamics and control of morphing aircraft, Thesis, Virginia Tech., 2005.

[36] B.L. Stevens, F.L. Lewis, Aircraft Control and Simulation, Wiley, New York, 2003.

[37] L. Fiorentini, A. Serrani, Adaptive restricted trajectory tracking for a non-minimum phase hypersonic vehicle model, Automatica 48 (7) (2012) 1248–1261.

[38] M.M. Polycarpou, P.A. Ioannou, A robust adaptive nonlinear control design, Automatica 32 (3) (1996) 423–427.

[39] K.P. Tee, S.S. Ge, E.H. Tay, Barrier Lyapunov functions for the control of output-constrained nonlinear systems, Automatica 45 (4) (2009) 918–927.

[40] B.B. Ren, S.S. Ge, K.P. Tee, T.H. Lee, Adaptive neural control for output feedback nonlinear systems using a barrier Lyapunov function, IEEE Trans. Neural Netw. 21 (8) (2010) 1339–1345.

[41] D. Liberzon, Switching in Systems and Control, Birkhauser, Boston, 2003.